Scanning Microscopy

Volume 8 | Number 2 Article 2

8-22-1994

Electronic Trap Microscopy - A New Mode for Scanning Electron Microscopy (SEM)

H. -J. Fitting
Rostock University, Germany

Th. Hingst
Rostock University, Germany

R. Franz
Rostock University, Germany

E. Schreiber
Rostock University, Germany

Scanning Microscopy, Vol. 8, No. 2, 1994 (Pages 165-174) 0891-7035/94$5.00+.25
Scanning Microscopy International, Chicago (AMF O'Hare), IL 60666 USA

ELECTRONIC TRAP MICROSCOPY - A NEW MODE FOR SCANNING ELECTRON MICROSCOPY (SEM)

H.-J. Fitting*, Th. Hingst, R. Franz, E. Schreiber

Physics Department, Rostock University,
Universitätsplatz 3, D-18051 Rostock, Germany

(Received for publication April 11, 1994, and in revised form August 22, 1994)

Abstract:

Insulating layers on conducting substrate are investigated by means of secondary electron field emission SEFE in a digital SEM. The kinetics of charge storage and release with time and temperature are controlled and recorded by an external computer.The evaluation is performed pixelwise with respect to electronic trap concentration n_{t0}, trap capture cross section σ_c and thermal activation energy E_t. Mapping of these trap parameters indicates hidden inhomogenities, defects and pre-treatments of the dielectric layers as well as the pattern of thermal bleaching and release of electrons. The latter ones appear as inhomogeneous processes starting with "blinking" centers and increasing their concentration with time and temperature.

KEY WORDS: Scanning electron microscopy, insulating layers, secondary electron emission, charging-up, Fowler-Nordheim injection, electronic traps, capture cross section, thermal activation energy, trap microscopy, defect mapping

* Address for correspondence:
H.-J. Fitting
Physics Department, Rostock University,
Universitätsplatz 3, D-18051 Rostock, Germany,
Phone No.: (+49)(381) 498 1646
Fax No.: (+49)(381) 498 1626

Introduction

Since the discovery of anomalous high secondary electron emission from porous MgO layers by Malter (1936), (Malter-effect), many attempts have been made to utilize field enhanced SEE (secondary electron emission) from insulating layers. Although manufacturing of stable Malter cathodes has not been successful, a steady interest in field-dependent SEE does exist. There were developments of electron beam storage screens, methods of electron beam charging and contacting, electret techniques and, of course, problems of charging-up prevention in electron spectroscopy and scanning electron microscopy (SEM), Seiler (1967) and Shulman and Friedrikhov (1977). The charging-up of insulating samples during electron excitation and emission is hardly avoidable. Consequently the resulting fields will affect the ratio of emitted electrons as well as their angular and energy distributions. An additional low energy electron exposure (rinsing) introduced by Salow (1940) often is used in order to fix the floating potential near the ground.

Our group set up experiments and a computer simulation of the self-consistent charging-up process in insulating layers during electron bombardment and secondary electron emission, Fitting et al. (1979). Besides spatial distributions of primary electron (PE) penetration, secondary electron (SE) generation and emission, hole (h) transport, trapping and Poole-Frenkel (PF) release of charges from located states, Fowler-Nordheim (FN) injection of electrons from the substrate and finally an eventual retarding field current j_R, due to a negatively biased first screening grid, were considered and taken into account.

Thus the total electronic current through the depth x is given by

$$j(x) = j_{PE} + j_{SE} + j_h + j_{PF} + j_{FN} + j_R \qquad (1)$$

Applying continuity and Poisson equation in planar geometry we get the field condition

$$\varepsilon_0 \varepsilon_r \frac{\partial}{\partial t} F(x) = j\,(x, t, \{F(x')\}) \qquad (2)$$

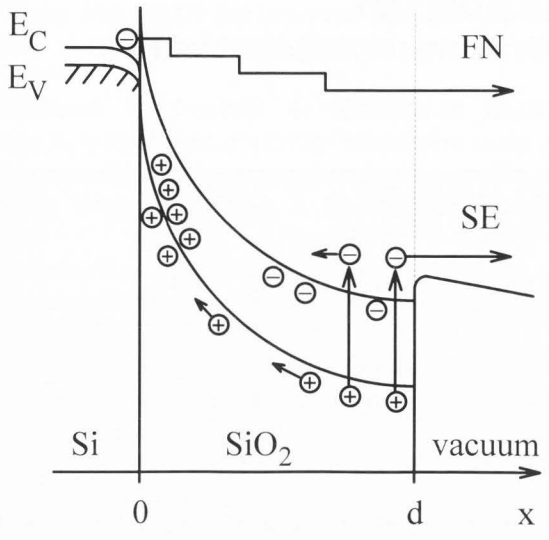

Fig. 1. Potential scheme for SEFE from a positively charged 100 nm SiO_2 layer on Si-substrate (SE: common SEemission; FN: Fowler-Nordheim part of SEE)

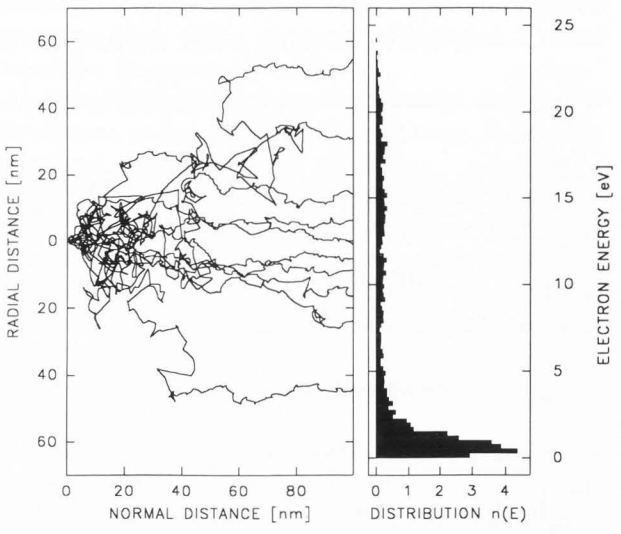

Fig. 2. Monte-Carlo trajectories and final energy distribution of Fowler-Nordheim injected electrons in SEFE regime as given in Fig. 1

and with an interation of eq.(2) the self-consistent charging-up j $\rightleftharpoons$ F, Fitting et al. (1979) and Fitting and Hecht (1988). Especially in case of positive charging-up of the insulating sample due to secondary electron yield $\sigma > 1$ for primary electron energies $E_0 < 2keV$, the Fowler-Nordheim injection from the substrate j_{FN} maintains the charge transport and limits the positive charge storage in the SE escape region near the surface, see Fig. 1 and 2.

Since the Fowler-Nordheim injection at the insulator-semiconductor interface is extremely field dependent

$$j_{FN} = AF^2 exp\left(-\frac{B}{F}\right) \tag{3}$$

we have used the FN-component for detection of smallest charge changes in dielectric layers on conducting substrate. Thus we created Secondary Electron Field Emission (SEFE) for electronic trap spectroscopy in thin insulating layers, see Fitting and Hecht (1988), and in combination with other methods, see Fitting et al. (1990).

The present paper will extend the trap spectroscopy by SEFE towards an image-providing mode of trap microscopy in SEMs.

Secondary Electron Field Emission (SEFE) Mechanisms

Secondary electron field emission (SEFE) as a new method for trap spectroscopy in insulating layers is based on extremely field-sensitive Fowler-Nordheim tunneling injection of electrons from conducting substrates into and through insulating layers, Fig. 1 and 2. Special Monte Carlo calculations have been carried out for these Fowler-Nordheim electrons injected from Si-substrate into the 100 nm SiO_2 layer and "seeing" a potential slope associated with an electric field as in Fig. 1.

The mechanisms of electron-phonon scattering, and impact ionization applied are described preliminary in Fitting (1993) but the detailled MC calculations are a part of the forthcoming PhD thesis of coworker E.S. In Fig. 2 the trajectories of penetration and emission are shown as well as the resulting FN-part of the SE energy distribution.

Obviously the SEFE tunneling probe works in SEE regions with SE yields $\sigma_{SE} > 1$ associated with high positive charging-up of the insulating layers and high field strength F towards the substrate interface. Any fluctuation of insulator charges Δ_ϱ will produce changes in the field strength, ΔF. Thus the alteration of the FN current eq.(3) may be expanded up to linear terms

$$j + \Delta j = A(F + \Delta F)^2 exp\left(-\frac{B}{F + \Delta F}\right) \simeq$$

$$\simeq j(F) + A\, exp\left(-\frac{B}{F}\right)(2F + B)\Delta F, \tag{4}$$

resulting in relative FN current changes as a function of field changes,

$$\frac{\Delta j}{j} \simeq \left(2 + \frac{B}{F}\right)\frac{\Delta F}{F}. \tag{5}$$

The tunneling parameters, here for the $Si - SiO_2$ interface have been estimated, Fitting et al. (1979) and Fitting and Hecht (1988), as follows:
$A \simeq 8.77 \cdot 10^{-8} A/V^2$
$B \simeq 2.26 \cdot 10^8 V/cm$
$F \simeq 7 \cdot 10^6 V/cm$, field strength operating point.
Inserting them we get a current-field relation
$\Delta j/j \simeq 34 \Delta F/F$.

The field in an open insulator-semiconductor structure towards the substrate is given by simple summation of charges ϱ_i:

$$F = \frac{1}{\varepsilon_0 \varepsilon_r} \sum_{i=1}^{n} \varrho_i \Delta x_i. \quad (6)$$

Relative charge changes around the operating point F then will be indicated by current changes

$$\frac{\Delta j}{j} \approx \left(2 + \frac{B}{F}\right) \frac{1}{F} \frac{1}{\varepsilon_0 \varepsilon_r} \int_0^d \Delta \varrho(x) dx. \quad (7)$$

ϱ is the spatial charge density of both polarities.

SEFE is performed by secondary electron excitation and hole generation simultaneously. Therefore, both charge carriers are offered to corresponding traps. Knowing capture and detrapping kinetics for electrons and holes in traps of concentration n_{t0} we get the time-related balance of occupied traps $n_t(t)$,

$$\frac{1}{e_0} \frac{d\varrho}{dt} = \frac{dn_t}{dt} = \frac{j_i}{e_0} \sigma_c (n_{t0} - n_t) - f exp\left(-\frac{E_t}{kT}\right) n_t. \quad (8)$$

j_i is the injected current of electrons or holes. On this way eq.(8) has been used already successfully for the evaluation of trap concentration n_{t0}, capture cross section σ_c and thermal activation energy E_t, even for both charge carriers electrons and holes, Fitting and Hecht (1988) and Fitting et al. (1990), Hecht and Fitting (1991).

Typical SEFE charge injection and thermal ejection cycles are presented in Fig. 4 and will be dicussed there. Details on an elementary SEFE apparatus are given in Hecht and Fitting (1991), however, the installation of SEFE in a SEM is the main subject of the present paper and will be discussed here for the first time.

Experimental Setup and Computer Controlling

The task was to perform electron and hole spectroscopy in thin insulating layers in a digital scanning electron microscope by means of the secondary electron field emission SEFE mode.

A digital Zeiss SEM DSM 960 provides a precise and reproducible electron beam system which is used for quantitative remote controlled SEFE measurements, Fig. 3. The primary electron energy E_0 can be varied also in the required low energy region from 0.3 to 2 keV while the beam current I_0 is held on a fixed value by changing the resolution settings. The time and temperature dependent secondary electron yield from insulating layers on (semi)conducting substrate is recorded by means of a digital image transfer interface and remote computer control. Charge storage parameters like capture cross section, trap concentration and thermal activation energy will be obtained in mapping presentation.

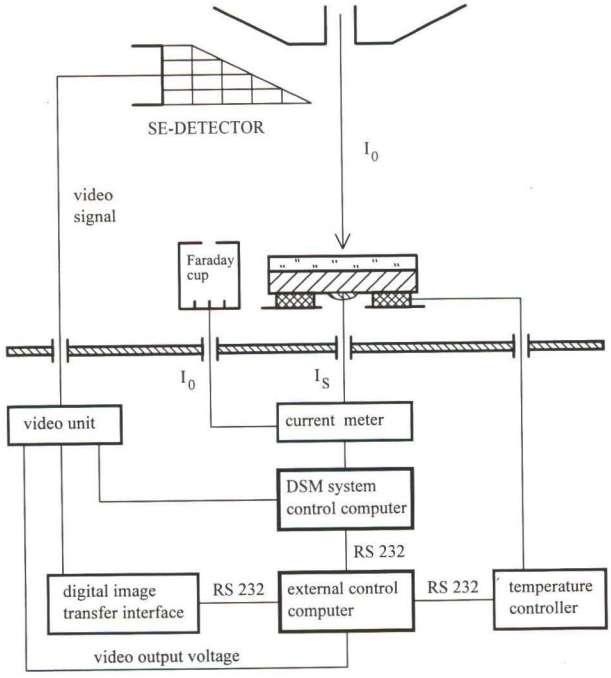

Fig. 3. Measurement system consisting of a digital SEM and an external computer control

Hardware configuration

The Zeiss DSM 960 is equipped with two serial interfaces (RS232) which are able to communicate with an external IBM-compatible PC. These interfaces can be programmed as a usual one (baud rate 150...9600; startbits 0, 1, 2; data bits 7, 8; parity even, odd, no). The electronics of the DSM with digital structure is controlled by microprocessors which observe the working states and execute the commands given by the front panel.

With an external PC one has access to all microprocessors (video computer, electron optics computer, stage control computer, vacuum system computer) and functions of the DSM via the internal system control computer (Fig. 3). The serial interface of the external PC has to be programmed to the same parameters as the DSM-interface. We use 4800 baud, 1 startbit, 8 data bits and no parity.

The computer program

The computer program RCDSM is written in Borland Pascal 7.0 and Turbo Vision 2.0 and comes up to the SAA-standard, Franz (1993). It can be used on all IBM-compatible PC with 2MB RAM, MS-DOS and at least three serial interfaces RS232, one for DSM control, one for digital image transfer (baud rate 115200) and one for the temperature controller. The program has a modular structure. Consequently, modules of the program can be used in other programs or extended versions.

An easy to handle menu and dialog system allows simple selection of DSM functions and parameter settings. Furthermore the program disposes of an on-line help system.

All commands given by the front panel to the system control computer can also be given by the external PC, but more quickly and more efficiently. The computer program performs routine tasks (X-Y-position; current measurements; high voltage, emission current, filament current; resolution and magnification settings; scan speed etc.). Furthermore there are some features which are not available by the front panel but only by remote control, for example the objective lens current settings or user defined X-Y-coordinates at the motorized stage. The computer program also controls the digital image transfer interface of the DSM to record SE images at definite times used later for pixel-wise evaluation, Franz (1993).

All working parameters can be read, saved and loaded later on. This guaranties a very good reproduction of the measurements. The most important parameters are permanently shown in a status box to provide quick information on the DSM working states.

SEFE-Curves: Integrated and Pixel-wise

SEFE-curves for the reason of trap spectroscopy as described by eq.(8) should be subdivided into two cycles:
a) Injection of carriers

The injection by electron bombardment results in inner Se and hole generation, i.e. charge carriers of both polarities are present and capture of these electrons and holes into traps n_t^-, n_t^+ becomes possible.

Then the changes of trap occupation $n_t(t)$ is indicated in real time by change of the measured total SE yield $\sigma_{SE} = \sigma(t) \propto n_t(t)$.

According to eq.(8) (left hand side), charge storage in traps with time follows a simple exponential saturation law

$$\sigma(t) = (\sigma_\infty - \sigma_0)\left[1 - exp\left(-\frac{j_i \sigma_c}{e_0} \cdot t\right)\right] + \sigma_0 =$$

$$= (\sigma_0 - \sigma_\infty) \cdot exp\left(-\frac{j_i \sigma_c}{e_0} \cdot t\right) + \sigma_\infty \qquad (9)$$

where the capture cross section σ_c can be calculated from the mean filling time $\tau = e_0/j_i\sigma_c$ of traps, acc. to eq.(9).
b) Thermal re-emission from traps

The heating-up of the sample with a constant heating rate $\mu = dT/dt$ causes thermal carrier emission from traps.

The release of trapped charges as a function of time is indicated by changes of σ_{SE} and the thermal activation energy E_t is accessible by evaluation of the right hand side term of eq.(8):

$$n_t = n_{t0}\, exp\left[-\frac{f}{\mu}\int_{T_0}^{T} exp\left(-\frac{E_t}{kT}\right)\right] dT \qquad (10)$$

In Fig. 4 typical SEFE charge injection and thermal ejection cycles are presented.

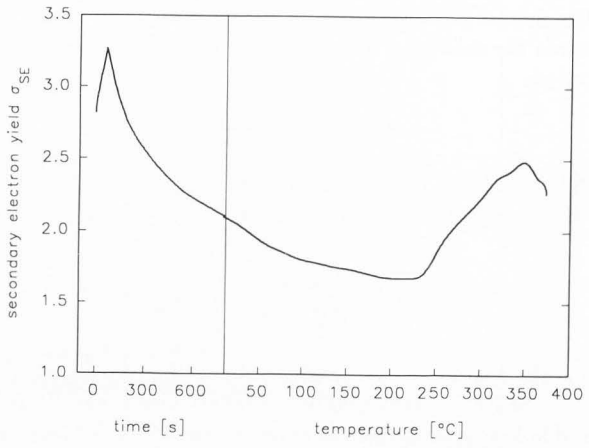

Fig. 4. Typical SEFE cycle with fast hole storage at the beginning, turnaround and long term electron incorporation with time; the thermal stimulation shows slight hole emission and then strong electron release between 250 and 350 ^oC; sample: 30 nm SiO_2 on Si

After very rapid positive charging-up at the beginning and fixing of FN-field strength of $F_0 \simeq 7MV/cm$ slower electron incorporation over the whole injection time $t = 1000s$ is observed, indicated by decrease of the SE rate according to eq.(9).

During the following thermal stimulation cycle with time-linear heating-up nearly to $T \simeq 400^oC$, holes and electrons are detrapped again, obviously from different centres at different temperatures. Superposed to the strong electron release between 250 and 350 ^oC a partial hole detrapping can be recognized by slight decays of the SEFE-curve plateaus. Such changes in the thermally stimulated SEFE yield have been evaluated by means of eq.(10) in detail, Fitting and Hecht (1988), and Fitting et al. (1990), Hecht and Fitting (1991), for obtaining the thermal activation energy E_t.

The logarithmic presentation of the injection cycle eq.(9)

$$ln(\sigma_t - \sigma_\infty) = ln(\sigma_0 - \sigma_\infty) - \frac{j_i}{e_0}\sigma_c \cdot t \qquad (11)$$

corresponding to trap concentrations

$$ln\, n_t = ln\, n_{t0} - \frac{j_i}{e_0}\sigma_c\, t \qquad (12)$$

allows to determine the overall trap concentration n_{t0} and the capture cross section σ_c by linear regression. We have done it for integrated SEFE curves as well as for each of the (512 x 512) pixels on the video screen and in the corresponding frame store as will be shown in the following:
c) Pixel-wise recording of the yield curves

The measurement is based on the quantitative relation between the total SE yield σ_{SE} (video signal from the SE detector) and the corresponding brightness of a pixel on the screen which is related to a video output voltage, see Fig. 3.

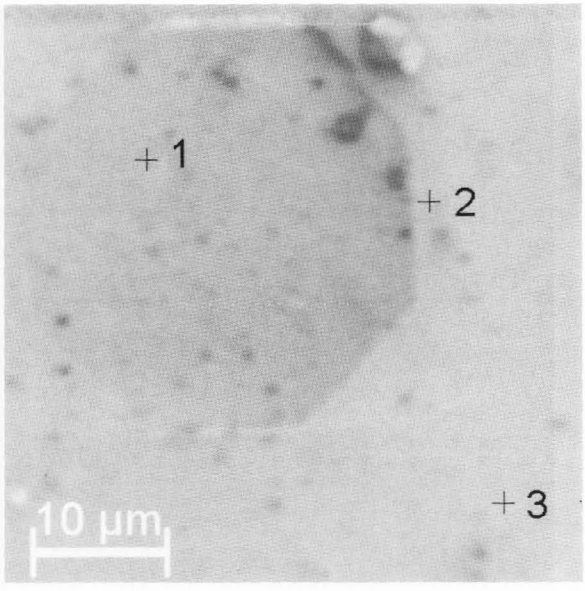

a)

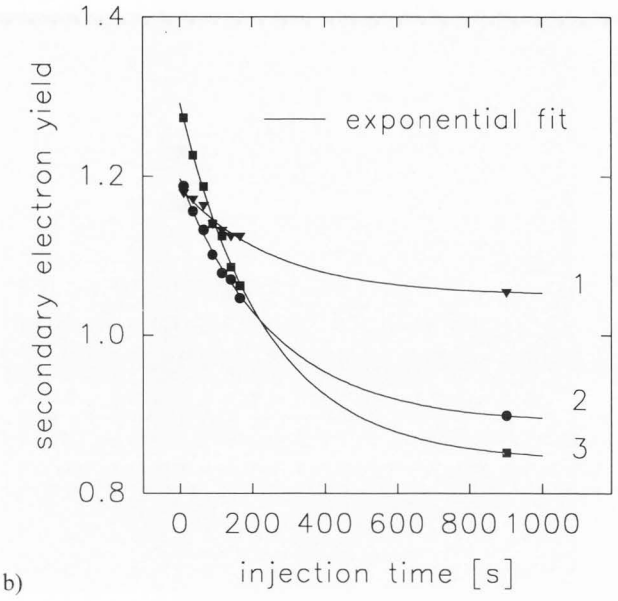

b)

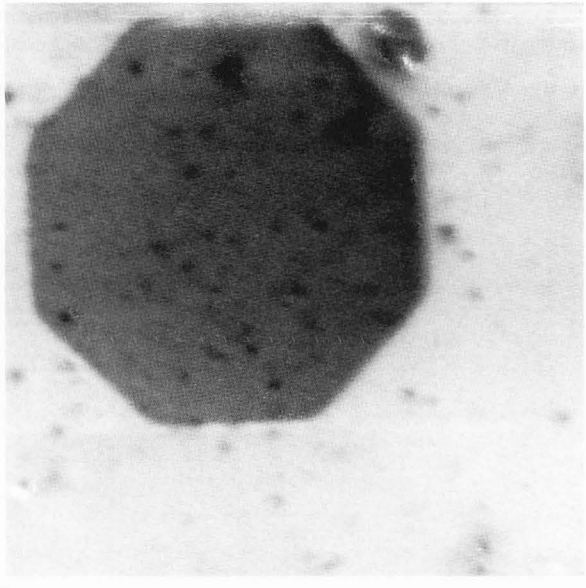

c)

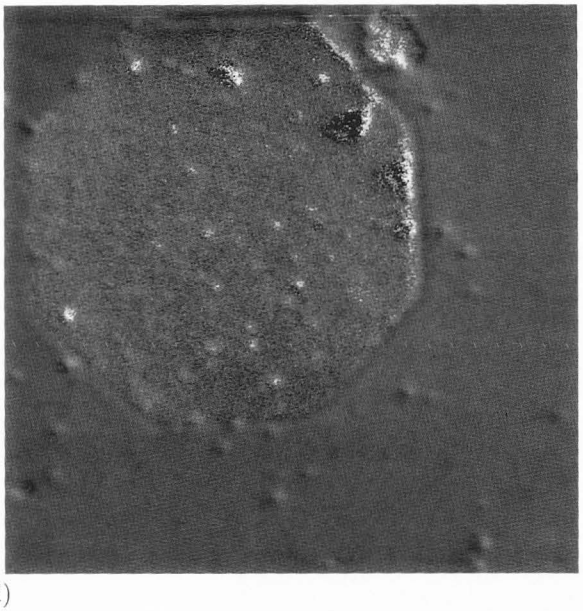

d)

Fig. 5. Floating Al-dot on 70 nm SiO_2 on Si
a) simple SE pattern with three positions marked (contrast enhanced +50%);
b) SEFE curves (electron storage) from pixels marked in a);
c) mapping of electron trap concentration n_{t0} (amplitude of SEFE curves);
d) mapping of electron trap capture cross section σ_c (slope of SEFE curves)

For that reason the SE detector has to be calibrated by means of manual contrast and brightness adjustment so that e.g. a SE yield range from 0 to 3 corresponds to the gray level range from 0 to 255.

The DSM 960 separates 256 gray levels on the screen which correspond to a video output voltage range between -0.49 V and +0.49 V, so that 256 different values of σ_{SE} per pixel can be distinguished.

At definite times the frame store is filled with the SE-image and the DSM 960 sends the contents of the frame store to an external PC via the internal digital image transfer interface.

For each of the (512 x 512) pixels of an image the external PC determines the time and temperature dependent SE yield and calculates the corresponding trap parameter, e.g. evaluation of eq.(12) by linear regression.

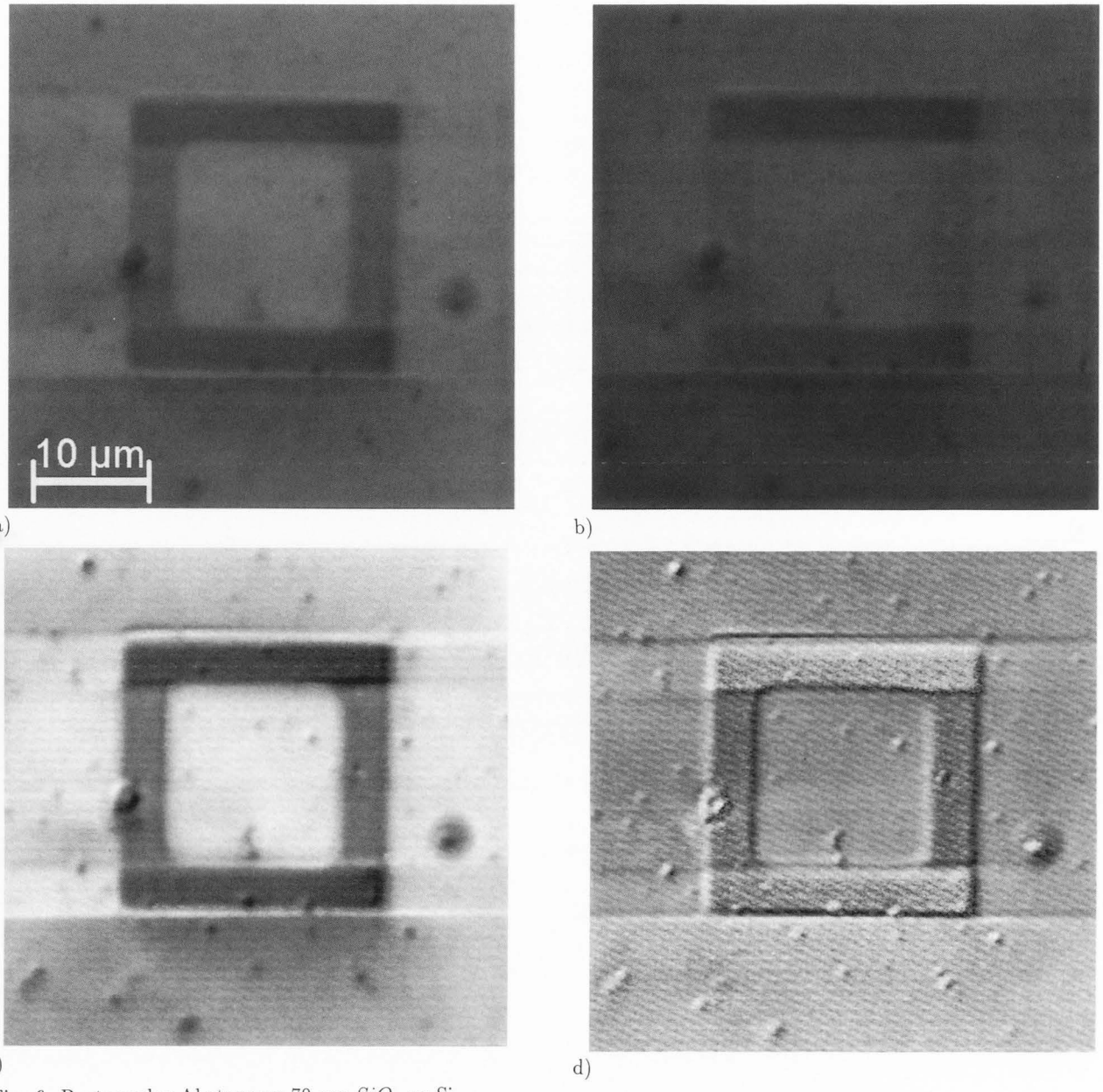

Fig. 6. Rectangular Al-stage on 70 nm SiO_2 on Si
a) and b) bleaching with time SE pattern after 10 s and 166 s, respectively (brightness enhanced +20%);
c) trap concentration mapping n_{t0};
d) electron capture cross section mapping σ_c

However, for the time being, we have still a limitation in pixel-wise determination of the thermal activation trap parameters caused by some deviation of the primary electron beam due to magnetic fields of the heater and by some thermal expansion of the heating-cooling-stage. Therefore, only one example for thermal imaging is given with Fig. 9 in the next chapter.

Contrary to that, the imaging of the trap filling could be performed in a very stable mode as expected. In Fig. 5a a very contrast-less topographic survey of a dot structure is shown by SE imaging after 10 s. For three different pixels marked by crossings the time dependent charge storage is plotted in the right hand part, Fig. 5b. We recognize different capture velocities by varied slopes as well as different

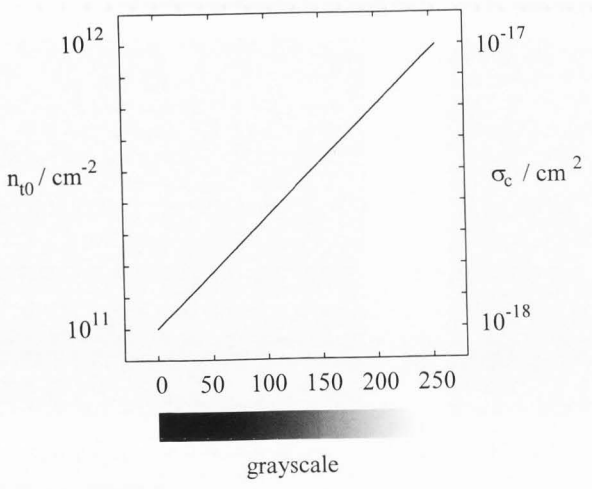

Fig. 7. Calibration of trap concentration n_{t0} and capture cross section σ_c with grayscale (0...255)

charge quantities given by the height of SEFE-curve alteration with time, e.g. $t_1 = 10s$, $t_8 = 900s$. Evaluation of each pixel intensity with respect to time and temperature will lead to a trap parameter mapping as to be seen in Fig. 5c and d. The trap concentration (Fig. 5c) on the octagon Al-dot is quite low, as expected, but the capture cross section σ_c of residual Al_2O_3 on the dot is higher than that of the SiO_2 field oxide. A more comprehensive description of trap mapping is considered in the following chapter.

SEFE Imaging – Electronic Trap Microscopy (ETM)

In the previous chapter we have seen that the odd problem of charging-up is not avoided in SEFE techniques, but in contrary, it is used especially for evidencing and imaging the electron and hole trap concentration n_{to}, the corresponding trap capture cross section σ_c and the activation energy E_t for thermal detrapping.

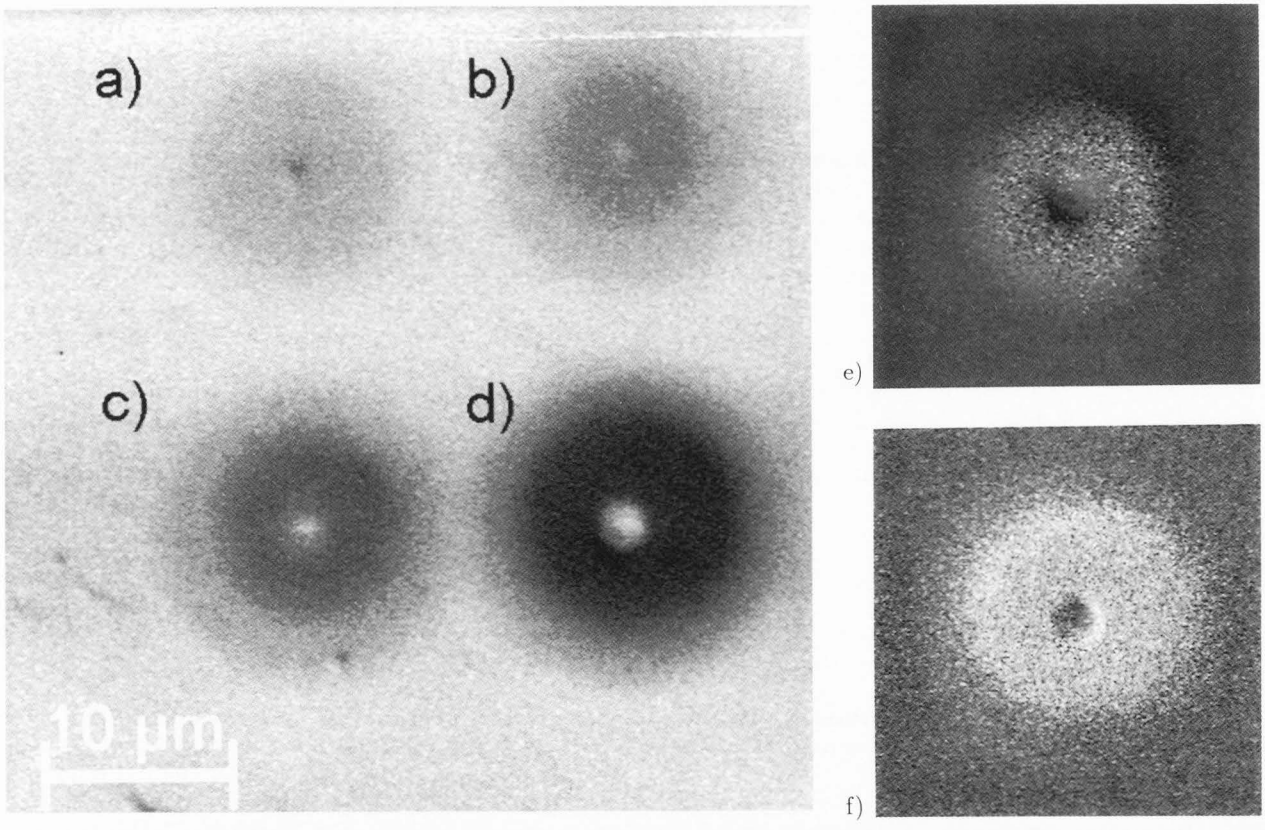

Fig. 8. High energy 30 keV electron bombardment in spot mode afterwards imaged by SEFE electrons 1 keV
a) 10 s, b) 50 s, c) 100 s, d) 500 s 30 keV bombardment time;
e) trap concentration n_{t0} and f) capture cross section σ_c mapping of 500 s bombardment pattern (d); (sample: 30 nm SiO_2 on Si)

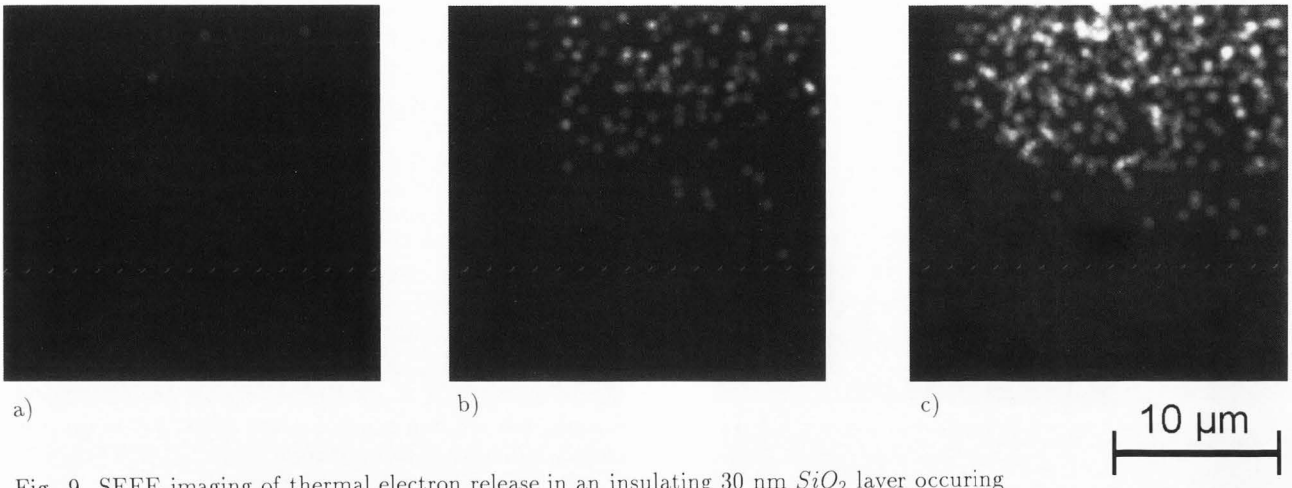

Fig. 9. SEFE imaging of thermal electron release in an insulating 30 nm SiO_2 layer occuring at local centres and increasing with temperature a) 150 $^{\circ}C$, b) 250 $^{\circ}C$, c) 350 $^{\circ}C$

Thus a usual SE-picture of an insulating sample in Fig. 5a and 6 a,b shows a slight contrast at the beginning of the initial exposure state, then rapidly bleaching to a gray and most structureless area. This charging-up behaviour in SEMs is known best. But by performing our SEFE techniques and imaging the electron trap concentration Fig. 5c and 6c and the electron trap capture cross section Fig. 5d and 6d we get a well-structured picture showing even all the hidden inhomogenities of the dielectric layer. In Fig.6 we see a rectangular Al-dot stage, dark, with almost no electronic traps, on an insulating SiO_2 layer on Si-substrate. Residual local states, i.e. some traps on the Al may be caused by its oxidation; probably a thin layer of 2 nm Al_2O_3 covers the surface, as already discussed for Fig.5. The 70 nm thick SiO_2 layer shows some local defects, here indicated mostly by lower trap concentration (dark) but in general with higher capture cross section (brighter). Moreover the defects themselves seem to be structured else. On the other hand the oxide horizontally left and right with respect to the stage shows another pre-treatment than the oxide fields in the upper and lower part of the picture area. It is evidenced by higher trap concentration in the middle part, however the capture cross sections appears almost non-changed.

Corresponding trap concentration n_t and capture cross sections σ_c have been calibrated with respect to the gray scale, as demonstrated in Fig. 7.

Another example for pre-treatment of the insulating layer is demonstrated in Fig. 8 a-d. The sample was bombarded with high energetic electrons $E_0 = 30$ keV in spot mode. The primary electron beam profile shows a small spot of several nm diameter with almost the full current intensity I_0 but then a ring of much lower current intensity surrounding the center spot with a radius of about 10 μm. This caustic ring of electron beam sources often appears.

After this high energy electron beam load the sample surface has been investigated by 1 keV - SEFE techniques. Clearly we see the centered spot-ring structure of the 30 keV pre-treatment beam profile as a dark pattern; Fig. 8a, i.e. the Fowler-Nordheim current is less than in other unirradiated regions. The electron trap concentration has been increased, but most of them are already occupied. Thus the number of traps which may be filled has been decreased, Fig. 8b. The capture cross section (Fig. 8c) of these 30 keV generated traps is smaller.

But the most interesting phenomena is the degradation "halo" around the centered primary spot inside the outer caustic ring, to be seen as a dark area in Fig. 8b,c. This effect is caused by backscattered electrons. For 30 keV-electrons the emerging area of backscattering from $SiO_2 - Si$ should be extended over several μm because the maximum penetration is 6 μm, Fitting (1974). The density of backscattered electrons is much less than the primary beam density therefore the degradation is increasing and spreading with bombardment time. With SEFE we are able to make visible the backscattering area, i.e. the density of electrons having escaped from the sample during the former 30 keV- bombardment.

The last experiment we should describe here is considering the thermal release of trapped electrons. First we have injected 1 keV electrons in a normal SEFE mode over 15 minutes. So the sample image became dark-gray. Then, by means of the sample heater a linear temperature increase with time was applied, Fig. 9 a - c. As we have already recognized in a general SEFE cycle, Fig. 4, a strong thermal release of trapped electrons is observed within the temperature interval 250 - 350 $^{\circ}C$. SEFE patterns of this process are shown in Fig. 9 a - c. At 150 $^{\circ}C$ several single bright pixels indicate the beginning of a pixel-wise bleaching, i.e. electron release at special initial points.

This process is enhanced with further temperature increase till 350 ^{o}C, the density of bleached bright pixels increases drastically showing that thermal activation and electron release are spontaneous local processes like a first-order phase transition.

We have seen the electron injection and trapping as homogeneously distributed over the oxide layer area, now the thermal release vice versa appears as pixel-wise distributed over the oxide layer. The latter behaviour seems to be typical for the thermally stimulated processes.

Conclusions

Secondary electron field emission (SEFE) is based on the extremely field-sensitive Fowler-Nordheim (FN) current injected from the substrate into positively charged insulating top layers maintaining the SE yield $\sigma_{SE} > 1$. This SEFE regime is obtained in general for primary electron (PE) energies $E_0 < 1.5keV$ and insulating top layers with thickness $d < 150nm$. The strong field dependence of the FN current allows to detect charge changes of $10^9 e_0/cm^2$ within the insulating top layer, Fitting and Hecht (1988). Thus a trap spectroscopy with respect to trap concentration n_{t0}, trap capture cross section σ_c, thermal activation energy E_t is performed by means of SEFE. This techniques has been installed into a SEM in order to get an image providing mapping of the above mentioned trap parameters n_{t0}, σ_c, E_t. For this reason the SEM is controlled by an external computer and time or temperature triggered images from the SEM frame store are transferred to the external PC. There, a data evaluation pixel-for-pixel as a function of time and temperature is carried out, providing a mapping of trap parameters. These patterns, e.g. for trap concentration/distribution n_{t0} or trap capture cross section σ_c, show inhomogenities and defects in insulating dielectric layers in a much more better view than normal SE or BE pattern do. The common crucial behaviour of charging-up and paling of SE images of insulating layers is used here especially for monitoring the kinetics of electronic traps, i.e. the capture process and the thermal release. First examples have been given in the present paper for trap concentration and capture cross section in SiO_2-layers on Si, making visible hidden defects, inhomogenities and pretreatments as well as the pixel-like beginning of thermal bleaching and release of incorporated charges (electrons) at temperatures 250-350 ^{o}C.

References

Fitting HJ. (1974). Transmission, energy distribution and SE excitation of fast electrons in thin solid films. Physica Status Solidi (a) 26; 525-535.

Fitting HJ. (1993). Vacuum emission of hot electrons from insulating and semiconducting films. J. Vac. Sci. Technol. B 11; 433- 436.

Fitting HJ, Hecht D. (1988). Secondary electron field emission - SEFE. Physica Status Solidi (a) 108; 265-273.

Fitting HJ, Glaefeke H, Wild W, Franke M, Müller W. (1979). Electron beam induced charge transport in SiO_2-layers. (in German) Experimentelle Technik der Physik 27; 13-24.

Fitting HJ, Magdanz P, Mehnert W, Hecht D, Hingst T. (1990). Charge trap spectroscopy in single and multiple layer dielectrics. Physica Status Solidi (a) 122; 297-309.

Franz R. (1993). Installation of secondary electron field emission in a digital SEM DSM 960. (in German). Master's Thesis, Rostock University.

Hecht D, Fitting HJ. (1991). Secondary electron field emission from SiO_2 and alternative insulating layers. (in German). Experimentelle Technik der Physik 39; 185-197.

Malter L. (1936). Anomalous SE, a new phenomenon. Phys. Rev. 49; 478-478.

Salow H. (1940). Über den Sekundäremissionsfaktor elektronenbestrahlter Isolatoren (On the secondary electron yield of electron-irradiated insulators). Zeitschrift für technische Physik 21; 8-15.

Seiler H. (1967). Einige aktuelle Probleme der SE (Some recent problems of the secondary emission). Zeitschrift für angewandte Physik 22; 249-263.

Shulman AR, Friedrikhov SA (1977). Secondary Emission Methods for Investigation of Solids. (in Russian) Nauka Press, Moscow.

Discussion with Reviewers

H. Niedrig: How do you distinguish experimentally between electron and hole trap concentration, how do you extract these quantities from the measuring data?
Authors: Trapped holes will charge up the dielectric layer positively, enhancing the FN-component and raising the SE yield; trapped electrons will decrease the SE yield. Both traps are neutral when unoccupied, i.e. in strong definition, they are donators in the first case and acceptors in the second one.

H. Niedrig: What other structures or processes could be well investigated by this imaging mode?
Authors: In general all microelectronic structures with insulating layers thinner than about 150 nm are suitable for this kind of electronic trap microscopy by means of SEFE. Furthermore processes like optical bleaching, photodepopulation and -injection of charge carriers, degradation of insulating layers should be accessible by this method.

J.T.Dickinson: During the heating process, is the primary electron beam off?
Authors: No, it is on, it is needed as the SEFE probe, although it can be operated with lower intensity j_0 in order to lower the recapture of charge carriers. Full description of capture and release is given by the balance eq.(8).

J.T.Dickinson: The $\Delta j/j$ which produces SEFE images is being modified by traps. How and where is the appropriate equation?
Authors: It is the direct equivalence of eq.(11) for SE yield σ_t and eq.(12) for the actual trap concentration n_t. Absolute values for n_t, n_{t0} are estimated by the linear expansion eq.(7).

F. Hasselbach: How long were the exposure times, e.g. of Fig.5? What is the resolution limit of this method? What is the smallest trap concentration or inhomogenity in surface charge you can see?
Authors: The exposure time is always given in the injection cycle, e.g. in Fig. 5b.
The SEFE injection current density for all presentations was fixed at $j_0 = 3 \cdot 10^{-5} A/cm^2$.
The resolution for this SEFE electronic trap microscopy corresponds in lateral resolution to the common SE-image-mode; in charge detection to $10^9\, e_0/cm^2$, see Fitting, and Hecht (1988).

F. Hasselbach: In Tübingen very thin (some nm) insulating layers were investigated emission microscopically by Jönsson et al. They were developing Metal-Insulator-Metal (MIM) cathodes (Vakuumtechnik 28 (1978), 66, Optik 77 (1987), 62). Is it possible to apply your method also to investigate these very thin tunneling junctions? On the other hand, would it be avantageous to do your measurements in an emission microscope where the whole image is formed simultaneously and not by scanning?
H. Niedrig: Do your results fit with the investigations of Jönsson and Niesche in Tübingen on MIM-cathodes?
Authors: The metallization of insulator surfaces prevents strong local electric fields and the Fowler-Nordheim current cannot be related to a certain position of the electron probe. Otherwise these metallized structures are well suitable for investigation in an emission microscope and MIS MIM-field emission pattern are obtained as refered above. Open, free insulating layers can be imaged by electron mirror microscopy (EMM) or low energy emission microscopy (LEEM) in an emission microscope arrangement too, but as well known, the lateral resolution is rather low.

F. Hasselbach: Is it possible to extract from Fig. 8 the current density of backscattered electrons quantitatively. If yes, agree your results concerning the spatial distributions of backscattered electrons with other experiments? Is contamination no problem after such intensive radiation by a 30 keV focused beam?
Authors: First of all, the drastic change in SEFE current $\sigma > 1$ is due to the FN component from the substrate. The responsible substrate interface to the insulator is well encapsuled and not exposed to contamination from the vacuum side. Also seggregation of certain species at the interface during the SEFE measurement seems not very probable, hence the incorporated charges should be responsible for controlling the FN-current and the SEFE signal.

Concerning the 30 keV irradiation, Fig. 8, impinging and backscattered high energy electrons will damage the sample, will generate electronic traps. A conclusion from this trap generation to backscattering densities of high energy electrons seems possible but has not yet been done quantitatively.